INTERNATIONAL JOURNAL FOR NUMERICAL METHODS IN FLUIDS, VOL. 13, 217–233 (1991)

THREE-DIMENSIONAL SPECTRAL APPROXIMATIONS TO STOKES FLOW BETWEEN ECCENTRICALLY ROTATING CYLINDERS

G. W. ROBERTS, A. R. DAVIES AND T. N. PHILLIPS

Department of Mathematics, The University College of Wales, Penglais, Aberystwyth, Dyfed SY23 3BZ, U.K.

SUMMARY

A three-dimensional spectral algorithm for the solution of Stokes flow between eccentrically rotating cylinders is described. Included in the model are pressure boundary conditions at the two ends of the finite length cylinders and the effect of a fluid line source on the inner cylinder. A comparison of results for the load and couple on the inner cylinder is made with those available from lubrication theory in the absence of a line source. Good agreement is shown for long, short and finite journal bearings when the various geometrical assumptions inherent in the lubrication analysis are satisfied.

KEY WORDS Spectral methods Journal bearing problem Stokes flow

1. INTRODUCTION

The journal bearing is an essential part of all internal combustion engines as a means of transferring the energy from the piston rods to the rotating crankshaft. It consists essentially of an inner cylinder (the journal), which is part of the crankshaft, and an outer cylinder (the bearing), which is at the end of the piston rod. In general, the two cylinders are eccentric and there is a lubricating film of oil separating the two surfaces. The addition of polymers to mineral (Newtonian) oils to minimize the variation of viscosity with temperature has the added effect of introducing strain-dependent viscosity and elasticity.

The physical problem has many complicating features which need to be modelled. It is a fully three-dimensional problem which therefore means that significant computational effort is required to solve the problem numerically. A non-linear constitutive equation is required to model the non-Newtonian lubricant. This means that, because of the non-linear relationship between stress and strain, the constitutive relations cannot be used to substitute for the components of stress in the field equations, unlike the corresponding Newtonian situation in which the stress may be computed at the end of the solution process. In the non-linear problem the stress may not be divorced from the velocity. In three dimensions there are six components of stress, which, along with the pressure and three velocity components, makes 10 variables which need to be calculated. To account for the oil flow through the bearing, consideration must be given to the oil source. This is a hole or groove in the inner journal, which therefore rotates in space. In addition, the system is subject to severe dynamic loading and has a complicated locus in space. Also, there is significant deformation of the bearing and journal[1] and extensive cavitation of the oil lubricant.

0271–2091/91/120217–17$08.50

Received April 1990
Revised August 1990

The following simplifying model is used.

1. The outer bearing is assumed stationary.
2. The inner journal is assumed to rotate about its own centre.
3. The oil is taken to be a Newtonian lubricant.
4. We assume steady state conditions, i.e. the forces and couple on the journal are calculated for fixed values of rotational speed and eccentricity.

It is usual to simplify the analysis by using Reynolds' lubrication equation suitably modified for the journal bearing geometry, and the further assumption of two-dimensional flow is widely used. We have chosen not to do this and have solved the full Stokes equations for the following two reasons. First, this work is the initial part of a project aimed at modelling the flow of non-Newtonian fluids. An extension of lubrication analysis to the non-Newtonian case was discounted on grounds of difficulty and lack of generality. Secondly, the results for Stokes flow are interesting in their own right since they highlight the effect of using a lubrication approximation and show in what limit there is a noticeable difference.

Figure 1 gives the geometrical details. The following variables are defined in terms of those shown in the figure: $D = 2R_B$, $c = R_B - R_J$ (the gap), $\varepsilon = e/c$ (eccentricity ratio) and $H = L/2$, where L is the length of the bearing in the axial direction (along the z-axis).

The main components of our algorithm are now described.

1. Results are obtained for Stokes flow, thus including terms in the governing equations which are ignored in a lubrication analysis.
2. The geometry of the problem is modelled exactly by use of cylindrical bipolar co-ordinates.
3. The three-dimensional nature is modelled by assuming periodic continuation in the axial direction and using a Fourier series expansion in z.

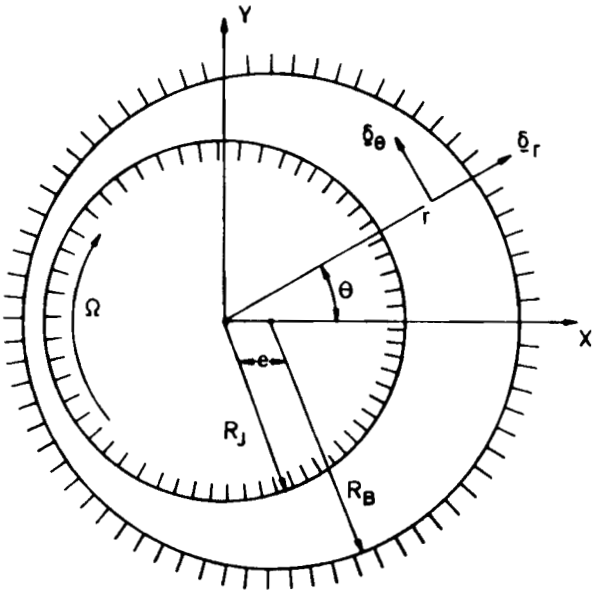

Figure 1. Geometry of eccentric cylinder model

4. A primitive variable mixed method is used,[2] i.e. a **u**, p, **T** formulation, so that the constitutive equation may be easily changed for the consideration of non-Newtonian models.
5. A spectral collocation method is used with the unknowns expanded as a tensor product of a Chebyshev and two Fourier series.
6. The oil source has been modelled by a uniform line source which approximates the rotation of a point source.

2. GOVERNING EQUATIONS AND BIPOLAR CO-ORDINATES

The following gives the general form of the continuity and momentum conservation equations for steady incompressible Stokes flow, where $\mathbf{u} = (u, v, w)$ and $\boldsymbol{\sigma}$ are the velocity and total (Cauchy) stress fields respectively:

$$\operatorname{div} \mathbf{u} = 0, \tag{1}$$

$$\operatorname{div} \boldsymbol{\sigma} = \mathbf{0}. \tag{2}$$

The total (Cauchy) stress may be expressed as $\boldsymbol{\sigma} = -p\mathbf{I} + \mathbf{T}$, where **T** is the extra stress (deviatoric stress) and p is the pressure.

The constitutive equation for a Newtonian fluid is given by

$$\mathbf{T} = 2\mu\mathbf{d}, \tag{3}$$

where μ is the viscosity and **d** is the rate-of-strain tensor defined by

$$\mathbf{d} = \tfrac{1}{2}(\nabla\mathbf{u} + \nabla\mathbf{u}^{\mathrm{T}}). \tag{4}$$

The cylindrical bipolar system (ξ, η, z) (see Figure 2) is given by

$$x = \frac{a \sinh \xi}{\chi}, \qquad y = \frac{a \sin \eta}{\chi}, \qquad z = z, \tag{5}$$

where $\chi = \cosh \xi + \cos \eta$ and a is a constant depending on ε, R_{J} and R_{B}.

Note that for two-dimensional problems the incompressibility condition (1) may be satisfied identically by use of a streamfunction formulation where the pressure is eliminated to leave the streamfunction and three components of extra stress as the unknown variables. In three dimensions the problem is less tractable since a scalar streamfunction does not exist and therefore a primitive variable formulation is used. For a mixed formulation there are 10 independent variables: three velocity components, the pressure and six components of extra stress.

For the journal bearing problem the following boundary conditions hold on the two cylindrical surfaces:

$$\begin{aligned}
&\mathbf{u} = \mathbf{0} && \text{on} \quad \xi = \xi_{\mathrm{B}},\\
&u = -\frac{Q}{2\pi R_{\mathrm{J}}}\delta(z) && \text{on} \quad \xi = \xi_{\mathrm{J}},\\
&v = \Omega R_{\mathrm{J}} && \text{on} \quad \xi = \xi_{\mathrm{J}},\\
&w = 0 && \text{on} \quad \xi = \xi_{\mathrm{J}},
\end{aligned} \tag{6}$$

where Q is the flow rate for the fluid source and δ is the delta function. The first of these statements enforces the no-slip condition for all the components of velocity on the outer bearing. The remaining three expressions give the velocity components at the inner journal: first the normal

velocity due to the fluid source, secondly the tangential velocity due to rotation and thirdly the no-slip condition in the axial direction.

The following gives the full set of Stokes equations (1)–(3) in terms of bipolar co-ordinates where $\chi = \cosh\xi + \cos\eta$ and $a =$ constant.

The conservation-of-mass equation is

$$\frac{\chi}{a}\frac{\partial u}{\partial \xi} + \frac{\chi}{a}\frac{\partial v}{\partial \eta} + \frac{\partial w}{\partial z} - \frac{u}{a}\sinh\xi + \frac{v}{a}\sin\eta = 0. \tag{7}$$

The three components of the equation of motion are

$$\begin{aligned}
\frac{\partial p}{\partial \xi} &= \frac{\partial T^{\xi\xi}}{\partial \xi} + \frac{\partial T^{\xi\eta}}{\partial \eta} + \frac{a}{\chi}\frac{\partial T^{z\xi}}{\partial z} + \frac{T^{\eta\eta} - T^{\xi\xi}}{\chi}\sinh\xi + 2\frac{T^{\xi\eta}}{\chi}\sin\eta,\\
\frac{\partial p}{\partial \eta} &= \frac{\partial T^{\xi\eta}}{\partial \xi} + \frac{\partial T^{\eta\eta}}{\partial \eta} + \frac{a}{\chi}\frac{\partial T^{\eta z}}{\partial z} + \frac{T^{\eta\eta} - T^{\xi\xi}}{\chi}\sin\eta - 2\frac{T^{\xi\eta}}{\chi}\sinh\xi,\\
\frac{\partial p}{\partial z} &= \frac{\chi}{a}\frac{\partial T^{z\xi}}{\partial \xi} + \frac{\chi}{a}\frac{\partial T^{\eta z}}{\partial \eta} + \frac{\partial T^{zz}}{\partial z} - \frac{T^{z\xi}}{a}\sinh\xi + \frac{T^{\eta z}}{a}\sin\eta.
\end{aligned} \tag{8}$$

The six constitutive equations are

$$\begin{aligned}
T^{\xi\xi} &= 2\mu\left(\frac{\chi}{a}\frac{\partial u}{\partial \xi} + \frac{v}{a}\sin\eta\right),\\
T^{\eta\eta} &= 2\mu\left(\frac{\chi}{a}\frac{\partial v}{\partial \eta} - \frac{u}{a}\sinh\xi\right),\\
T^{zz} &= 2\mu\frac{\partial w}{\partial z},\\
T^{\xi\eta} &= \mu\left(\frac{\chi}{a}\frac{\partial v}{\partial \xi} - \frac{u}{a}\sin\eta + \frac{\chi}{a}\frac{\partial u}{\partial \eta} + \frac{v}{a}\sinh\xi\right),\\
T^{\eta z} &= \mu\left(\frac{\chi}{a}\frac{\partial w}{\partial \eta} + \frac{\partial v}{\partial z}\right),\\
T^{z\xi} &= \mu\left(\frac{\chi}{a}\frac{\partial w}{\partial \xi} + \frac{\partial u}{\partial z}\right).
\end{aligned} \tag{9}$$

3. SPECTRAL APPROXIMATION

The scheme used for the numerical solution of the equations is based on spectral methods which are well known to give accurate results for a small number of degrees of freedom as compared with finite difference and finite element techniques (see Reference 3, for example). This was an important consideration for the ultimate aim of a full three-dimensional transient non-linear code.

The equations are formulated in cylindrical bipolar co-ordinates (see Figure 2) and solved using a spectral collocation scheme with each variable expanded as a tensor product of two Fourier and one Chebyshev series. The programme gives the two-dimensional solution for the infinitely long journal as a special case and includes the effect of the fluid source for the finite bearing. The six extra-stress (deviatoric-stress) components are expanded independently in order to facilitate the extension of the scheme to elastic fluids. The solution of the resulting matrix equations gives the

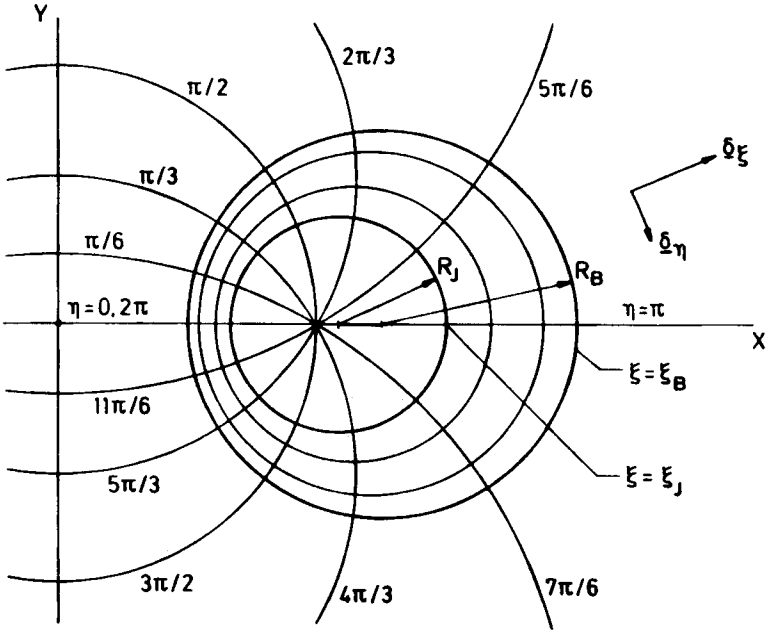

Figure 2. Bipolar co-ordinate system

spatial distribution of the three components of velocity, the pressure and the six components of extra stress. The pressure and normal extra-stress components are then integrated over the journal surface to obtain the load, and the tangential extra-stress component is integrated to obtain the torque.

Physically, the finite journal is open to the atmosphere at both ends so that $p = 0$ there, and the flow is symmetric about the middle of the journal so that u and v are symmetric functions of z and w is an antisymmetric function of z.

To circumvent the unknown velocity fields at the free boundaries at $z = \pm L/2$, we treat the problem of end seepage by an artificial periodic continuation of all variables in the z-direction with period $2L$. To conserve mass when considering the oil source, it is sufficient to introduce an infinite array of line sources and sinks in the periodically continued u-component which is symmetric about $L/2$. Also the v-component is symmetric about $L/2$ whilst the w-component is antisymmetric about $L/2$. This leads to an odd cosine series for u and v and an odd sine series for w. The expansions for the components of extra stress follow from the constitutive equations. The components of extra stress $T^{\eta z}$ and $T^{z\xi}$ are sine series in z whilst the remainder are cosine series. This structure is totally consistent with the physical boundary conditions on the journal.

The 10 variables are each expanded in terms of two Fourier and one modified Chebyshev series. The general expansion for a variable $\phi(\xi, \eta, z)$ is of the form

$$\phi(\xi, \eta, z) = \sum_{k=0}^{K} \sum_{m=-M/2}^{M/2} \sum_{n=0}^{N} \hat{\phi}_{kmn} T_k(\xi) \exp(im\eta) \begin{Bmatrix} \cos(n\pi z/L) \\ \sin(n\pi z/L) \end{Bmatrix}, \tag{10}$$

where $\hat{\phi}_{kmn}$ are expansion coefficients. The modified Chebyshev polynomials are defined on the interval $[\xi_B, \xi_J]$ by a transformation from $[-1, 1]$ to $[\xi_B, \xi_J]$ given by $\xi = (\xi_J - \xi_B)(x-1)/2 + \xi_J$.

Because of spurious high-pressure modes,[3] the pressure expansion omits the highest-order Chebyshev polynomial. The expansions are substituted in the differential equations and the orthogonality of the Fourier series in z is utilized to obtain reduced problems for each Fourier mode. The boundary conditions for each mode are given by the Fourier projection of the physical ones. Lanczos[4] σ-factors may be used to give a more rapidly convergent Fourier series for the delta function which represents the line source. This is also referred to as smoothing. Taking the general expansion to be

$$\phi(\xi, \eta, z) = \sum_{n=0}^{N} \tilde{\phi}_n(\xi, \eta) \begin{Bmatrix} \cos(n\pi z/L) \\ \sin(n\pi z/L) \end{Bmatrix}, \tag{11}$$

the Fourier components of the boundary conditions are given by

$$\tilde{\phi}_n(\xi_B, \eta) = \sigma(n\pi/N) \int_0^L \phi(\xi_B, \eta, z) \begin{Bmatrix} \cos(n\pi z/L) \\ \sin(n\pi z/L) \end{Bmatrix} dz, \tag{12}$$

where

$$\sigma(\theta) = 1 \tag{13}$$

for the standard Fourier components and

$$\sigma(\theta) = \frac{\sin\theta}{\theta} \tag{14}$$

when Lanczos smoothing is used. The smoothing function $\sigma(\theta)$ in (14) is a non-negative function on $[-\pi, \pi]$ with $\sigma(\theta) \simeq 1$ for $|\theta| \simeq 0$ and $\sigma(\theta) \to 0$ as $|\theta| \to \pi$.

For the velocity components this gives, when $\sigma(\theta) = 1$,

$$\mathbf{u}_n = \mathbf{0} \qquad \text{on} \quad \xi = \xi_B, \tag{15}$$

$$\tilde{u}_n = -\frac{Q}{\pi R_J L} \qquad \text{on} \quad \xi = \xi_J, \quad n \text{ odd}, \tag{16}$$

$$\tilde{u}_n = 0 \qquad \text{on} \quad \xi = \xi_J, \quad n \text{ even}, \tag{17}$$

$$\tilde{v}_n = \frac{4\Omega R_J}{n\pi}(-1)^{(n-1)/2} \qquad \text{on} \quad \xi = \xi_J, \quad n \text{ odd}, \tag{18}$$

$$\tilde{v}_n = 0 \qquad \text{on} \quad \xi = \xi_J, \quad n \text{ even}, \tag{19}$$

$$\tilde{w}_n = 0 \qquad \text{on} \quad \xi = \xi_J. \tag{20}$$

The problem for each Fourier z-mode is collocated to give an algebraic system of equations for the unknown expansion coefficients. The collocation points are spaced linearly in the circumferential direction ($\eta_j = 2\pi j/(M+1)$, $0 \leqslant j \leqslant M$). In the radial direction the collocation points are located at the extrema ($x_j = \cos(\pi j/K)$, $0 \leqslant j \leqslant K$) or zeros ($x_j = \cos[\pi(j+\frac{1}{2})/K]$, $0 \leqslant j \leqslant K-1$) of the Chebyshev polynomial of highest degree used in the expansion. These sets of points are known as the Gauss–Lobatto–Chebyshev and Gauss–Chebyshev points respectively. In a collocation method the choice of collocation points is crucial. In spectral methods they are always chosen to be the nodes of a Gaussian quadrature rule for two reasons. First, the Lagrange interpolating polynomial which interpolates the data at these nodes possesses good approximating properties. Secondly, for linear problems the collocation method may be shown to be equivalent to a variational formulation of the problem when the same quadrature rule is used to approximate the integrals appearing in this formulation. Following Canuto *et al.*,[3] the continuity and momentum equations are collocated at the Gauss–Chebyshev and interior Gauss–Lobatto–Chebyshev points

respectively. If the continuity and momentum equations are both collocated at the Gauss–Lobatto–Chebyshev points, then the linear system for the expansion coefficients is underdetermined. The velocity boundary conditions are collocated at the extreme Gauss–Lobatto–Chebyshev points. In addition, the constitutive equations are collocated at all the Gauss–Lobatto–Chebyshev points.

For the long (2D) bearing calculation ($n=0$) the pressure mode $\hat{p}_{000}$ represents the mean value of the pressure and has no effect upon the velocity since its gradient vanishes. It is introduced into the modified continuity equation

$$\operatorname{div}\mathbf{u} = \hat{p}_{000} \tag{21}$$

to balance the number of unknowns and collocation points. This avoids the ill-defined and apparently highly sensitive alternative of not collocating one of the equations at a chosen point. Integrating (21) over the interior of the journal bearing and using the divergence theorem on the left-hand side of (21), we can show that the volume integral of $\hat{p}_{000}$ is zero, from which it follows that $\hat{p}_{000}$ is identically zero.

The matrix equation for each z-component subproblem is solved by a direct method using the NAG routine F04ADF which uses Crout's factorization followed by back-substitution.

After solving the system, the load $\mathbf{F}$ and torque C on the journal may be calculated as

$$\mathbf{F} = -\int\!\!\int_{\xi=\xi_J} \boldsymbol{\sigma}\cdot\hat{\mathbf{n}}\,\mathrm{d}S = -\int\!\!\int_{\xi=\xi_J} \begin{pmatrix} T^{\xi\xi}-p \\ T^{\eta\xi} \\ T^{z\xi} \end{pmatrix} \mathrm{d}S, \tag{22}$$

$$C = -R_J \int\!\!\int_{\xi=\xi_J} \boldsymbol{\sigma}\cdot\hat{\mathbf{t}}\,\mathrm{d}S = -R_J \int\!\!\int_{\xi=\xi_J} T^{\eta\xi}\,\mathrm{d}S, \tag{23}$$

where $\hat{\mathbf{n}}$ and $\hat{\mathbf{t}}$ are the unit vectors normal and tangential to the journal. Expressing the integrals in terms of bipolar co-ordinates and transforming the forces to Cartesian components gives

$$F_X = -\int_{-H}^{H}\int_0^{2\pi} \left((T^{\xi\xi}-p)_J \frac{1+\cosh\xi_J\cos\eta}{\chi_J} + T^{\eta\xi}_J \frac{\sinh\xi_J\sin\eta}{\chi_J} \right) \frac{a}{\chi_J}\,\mathrm{d}\eta\,\mathrm{d}z, \tag{24}$$

$$F_Y = -\int_{-H}^{H}\int_0^{2\pi} \left((T^{\xi\xi}-p)_J \frac{-\sinh\xi_J\sin\eta}{\chi_J} + T^{\eta\xi}_J \frac{1+\cosh\xi_J\cos\eta}{\chi_J} \right) \frac{a}{\chi_J}\,\mathrm{d}\eta\,\mathrm{d}z, \tag{25}$$

$$F_Z = -\int_{-H}^{H}\int_0^{2\pi} T^{z\xi}_J \frac{a}{\chi_J}\,\mathrm{d}\eta\,\mathrm{d}z, \tag{26}$$

$$C = -R_J \int_{-H}^{H}\int_0^{2\pi} T^{\eta\xi}_J \frac{a}{\chi_J}\,\mathrm{d}\eta\,\mathrm{d}z, \tag{27}$$

where $f_J \equiv f(\xi_J, \eta, z)$. The expansions are substituted in the integrals, which are then calculated analytically using contour integration. The details are given in Appendix I.

4. LUBRICATION THEORY

Results from the Stokes flow calculations without the inclusion of the line source ($Q=0$) are compared with those from lubrication theory for full film conditions. When the gap is small compared with other dimensions, it is possible to perform an order-of-magnitude analysis on the full Navier–Stokes equation. This results in Reynolds' equation when small terms are ignored. The

analysis neglects inertial terms, so that lubrication theory flow is a Stokes flow with further simplifying assumptions.

4.1. Finite bearing

The standard form of Reynolds' equation is

$$\frac{\partial}{\partial y}\left(h^3\frac{\partial p}{\partial y}\right)+\frac{\partial}{\partial z}\left(h^3\frac{\partial p}{\partial z}\right)=6U\mu\frac{\partial h}{\partial y}, \tag{28}$$

where p, h and μ are the pressure, film thickness and viscosity of the lubricant respectively and U is the relative velocity of bearing surfaces.

In journal bearings, y and z are taken along the circumferential and axial directions respectively. Note that the pressure is assumed constant across the gap, i.e. $\partial p/\partial x = 0$. For the journal bearing, if $y = R_J\theta$, the height of the gap is approximated by $h = c(1 + \varepsilon\cos\theta)$, which is sufficiently accurate if $c/R_J \ll 1$.

Omitting the subscript for R_J, introducing dimensionless variables $\theta = y/R$, $Z = z/2L$ and noting that $U = \Omega R$, Reynolds' equation becomes

$$\frac{\partial}{\partial\theta}\left((1+\varepsilon\cos\theta)^3\frac{\partial P}{\partial\theta}\right)+\left(\frac{R}{2L}\right)^2\frac{\partial}{\partial Z}\left((1+\varepsilon\cos\theta)^3\frac{\partial P}{\partial Z}\right)=-6\mu\Omega R^2\frac{\varepsilon}{c^2}\sin\theta. \tag{29}$$

The boundary conditions on P are

$$P(-\pi, Z)=P(\pi, Z), \qquad \frac{\partial P}{\partial\theta}(-\pi, Z)=\frac{\partial P}{\partial\theta}(\pi, Z), \tag{30}$$

$$P(\theta, 1)=0, \qquad P(\theta, -1)=0. \tag{31}$$

The Cartesian components F_X and F_Y of the load and the torque C on the journal are given by

$$F_X=\int_{-H}^{H}\int_0^{2\pi} p\cos\theta\, R\,\mathrm{d}\theta\,\mathrm{d}z, \tag{32}$$

$$F_Y=\int_{-H}^{H}\int_0^{2\pi} p\sin\theta\, R\,\mathrm{d}\theta\,\mathrm{d}z, \tag{33}$$

$$C=R\int_{-H}^{H}\int_0^{2\pi}\mu\frac{\partial v}{\partial z}R\,\mathrm{d}\theta\,\mathrm{d}z=\frac{2\pi\mu L\Omega R^3}{c\sqrt{(1-\varepsilon^2)}}+\frac{F_Y e}{2}. \tag{34}$$

Note that the pressure gradient terms are retained in both the circumferential and axial directions. Tao[5] obtained an analytical solution using Heun functions. There are several numerical solutions—a finite difference technique is used by Cameron[6] and Tanner[7] uses a Galerkin method.

We use a pseudospectal collocation solution scheme where the pressure is expanded as the tensor product of a Fourier series in θ and a Chebyshev series in Z, i.e.

$$p(\theta, Z)=\sum_{m=-M/2}^{M/2}\sum_{n=0}^{N}\hat{p}_{mn}\exp(im\theta)\,T_n(Z), \tag{35}$$

where $\hat{p}_{mn}$ are expansion coefficients. The collocation points are spaced linearly in the circumferential direction ($\theta_j = 2\pi j/M$, $0 \leqslant j \leqslant M-1$) and at the Gauss–Lobatto–Chebyshev points in the axial direction ($Z_j = \cos(\pi j/N)$, $0 \leqslant j \leqslant N$). The expansion for p automatically satisfies the periodic

boundary conditions (30). The differential equation (29) is collocated at the internal Gauss–Lobatto–Chebyshev points and the zero-pressure boundary condition (31) is collocated at the extreme Gauss–Lobatto–Chebyshev points. The resulting algebraic system is solved using a direct method to give the values of the pressure field at the collocation points. The load **F** and torque C on the journal may then be calculated by substituting the expansion for pressure in (32)–(34). The details are given in Appendix II.

4.2. Long bearing

Assume that the effect of the side boundary conditions is negligible and that the flow is two-dimensional. The pressure distribution obtained from this approximation is accurate only for the central plane of a real bearing with $L/D \geqslant 5$. When $\partial p/\partial Z$ is neglected, Reynolds' equation can be solved analytically to give

$$p - p_0 = \frac{6\mu\Omega R^2}{c^2} \frac{\varepsilon \sin\theta(2+\varepsilon\cos\theta)}{(2+\varepsilon^2)(1+\varepsilon\cos\theta)^2}, \tag{36}$$

$$F_X = 0, \tag{37}$$

$$F_Y = \frac{12\pi\mu L\Omega R^3\varepsilon}{c^2\sqrt{(1-\varepsilon^2)(2+\varepsilon^2)}}, \tag{38}$$

$$C = \frac{2\pi\mu L\Omega R^3}{c\sqrt{(1-\varepsilon^2)}} + \frac{F_Y e}{2}. \tag{39}$$

4.3. Short bearing

Assume that the side boundary conditions give rise to a much larger pressure gradient than that due to the rotation of the journal. Results are fairly accurate for $L/D \leqslant 1/5$. If $\partial p/\partial\theta$ is neglected, Reynolds' equation can again be solved analytically to give

$$p - p_0 = \frac{3\mu\Omega\varepsilon\sin\theta}{c^2(1+\varepsilon\cos\theta)^3}\left(\frac{L^2}{4} - z^2\right), \tag{40}$$

$$F_X = 0, \tag{41}$$

$$F_Y = \frac{\pi\mu L^3\Omega R\varepsilon}{2c^2(1-\varepsilon^2)^{3/2}}, \tag{42}$$

$$C = \frac{2\pi\mu L\Omega R^3}{c\sqrt{(1-\varepsilon^2)}} + \frac{F_Y e}{2}. \tag{43}$$

5. RESULTS WITHOUT FLUID SOURCE

Results are presented for values of the expansion parameters in (10) of $K = M = 8$, $N = 7$. Higher values of these parameters were used and essentially similar values of the load and torque were obtained, which shows that the numerical solution has converged with mesh refinement.

We concentrate on a bearing of typical size under typical conditions:

$\Omega = 250$ rad s^{-1} (≈ 2500 rpm)

$D = 62{\cdot}5$ mm (2·5 in)

$L/D = 10, 5, 2{\cdot}5, 1, 0{\cdot}5, 0{\cdot}1$

$(L = 62{\cdot}5, \ldots, 6{\cdot}25$ mm)

$c = 0{\cdot}4$ mm (0·01575 in)

$\varepsilon = 0{\cdot}1, 0{\cdot}2, \ldots, 0{\cdot}9, 0{\cdot}95, 0{\cdot}99$

$(e = 0{\cdot}04, 0{\cdot}08, \ldots, 0{\cdot}36, 0{\cdot}38, 0{\cdot}395$ mm)

$\mu = 5$ mPa s.

Note that $c/D \approx 1/160$ so that lubrication theory should give accurate results for Newtonian flows. The axial length L was varied to give values of L/D between 10/1 and 1/10, and e was varied to give eccentricities $\varepsilon = e/c$ between 0·1 and 0·99. The different eccentricities give rise to shear rates of $\dot{\gamma} \approx 2{\cdot}6 \times 10^4\ \mathrm{s}^{-1}$ for $\varepsilon = 0{\cdot}1$ and $\dot{\gamma} \approx 1{\cdot}6 \times 10^6\ \mathrm{s}^{-1}$ for $\varepsilon = 0{\cdot}99$.

The Stokes solutions give $F_X = 0$ and $F_Z = 0$, as for lubrication theory.

Tables I–III give the values for normal load F_Y and torque C given by the 3D Stokes solution, finite lubrication theory, short bearing approximation and long bearing approximation for L/D ratios of 1/10, 1/1 and 10/1 respectively. Comparison of results from the 2D Stokes solution with those given by the long bearing lubrication approximation shows very close agreement for all eccentricities, so the Stokes 2D results are not tabulated.

The calculation of F_Y for the 3D Stokes solution (25) includes the extra-stress components. This has negligible effect when $L/D \geqslant 1/5$, but has increasing influence for short bearings. For $L/D = 1/10$, Table I shows two values of F_Y for the 3D Stokes solution: F_Y(total) is calculated by (25) whereas F_Y(pressure) is calculated by integrating the pressure only. The values of F_Y (pressure) agree with those given by finite lubrication theory, but F_Y (total) is less for small eccentricities and bigger for large eccentricities.

For $L/D = 10/1$, Table III shows that the long lubrication approximation gives good results for all eccentricities. Likewise, for $L/D = 1/10$ the short lubrication approximation gives good results except when $\varepsilon \geqslant 0{\cdot}95$, when F_Y is overestimated. As was expected, the short and long lubrication approximations were found to be accurate only for $L/D \leqslant 1/5$ and $L/D \geqslant 5/1$ respectively.

Figure 3 shows the pressure distribution within the annulus for the case $L/D = 1/10$ and $\varepsilon = 0{\cdot}9$. The pressure field is symmetrical about the line joining the centres of the cylinders, which therefore gives a load on the journal in the vertical direction.

Figure 4 shows the circumferential velocity for the case $L/D = 1/10$ and $\varepsilon = 0{\cdot}9$. This shows recirculation regions in the area of largest gap which cannot be predicted by lubrication theory, but agrees with previous results for Stokes flow.[8]

Numerical experiments showed that discrepancies arise between the lubrication and Stokes results for increasing values of c/R, which is to be expected since the lubrication theory assumes $c/R \ll 1$.

6. EFFECT OF FLUID SOURCE

An estimated value for the flow rate of fluid through the journal bearing of $5 \times 10^{-6}\ \mathrm{m}^3\,\mathrm{s}^{-1}$ has been taken from the literature. When this source strength is distributed around the journal, a large pressure is produced in the region of smallest gap. Although F_Y remains the same as in the sourceless case, F_X is no longer zero and is comparable in magnitude to F_Y (see Table IV). Therefore both the magnitude and direction of the total load are substantially modified. This is not physically realistic since it means that fluid enters via the oil hole even at regions of high pressure within the annulus.

Table I. Results for $L/D = 1/10$

	Stokes 3D			Finite lub		Short lub		Long lub	
ε	F_Y(total)	F_Y(pressure)	C	F_Y	C	F_Y	C	F_Y	C
0·1	$0{\cdot}39 \times 10^{-2}$	$0{\cdot}93 \times 10^{-2}$	$0{\cdot}38 \times 10^{-2}$	$0{\cdot}95 \times 10^{-2}$	$0{\cdot}38 \times 10^{-2}$	$0{\cdot}95 \times 10^{-2}$	$0{\cdot}38 \times 10^{-2}$	$0{\cdot}28 \times 10^{1}$	$0{\cdot}38 \times 10^{-2}$
0·2	$0{\cdot}84 \times 10^{-2}$	$0{\cdot}20 \times 10^{-1}$	$0{\cdot}39 \times 10^{-2}$	$0{\cdot}20 \times 10^{-1}$	$0{\cdot}38 \times 10^{-2}$	$0{\cdot}20 \times 10^{-1}$	$0{\cdot}38 \times 10^{-2}$	$0{\cdot}56 \times 10^{1}$	$0{\cdot}40 \times 10^{-2}$
0·3	$0{\cdot}14 \times 10^{-1}$	$0{\cdot}32 \times 10^{-1}$	$0{\cdot}40 \times 10^{-2}$	$0{\cdot}32 \times 10^{-1}$	$0{\cdot}39 \times 10^{-2}$	$0{\cdot}32 \times 10^{-1}$	$0{\cdot}39 \times 10^{-2}$	$0{\cdot}85 \times 10^{1}$	$0{\cdot}44 \times 10^{-2}$
0·4	$0{\cdot}23 \times 10^{-1}$	$0{\cdot}48 \times 10^{-1}$	$0{\cdot}41 \times 10^{-2}$	$0{\cdot}48 \times 10^{-1}$	$0{\cdot}41 \times 10^{-2}$	$0{\cdot}49 \times 10^{-1}$	$0{\cdot}41 \times 10^{-2}$	$0{\cdot}11 \times 10^{2}$	$0{\cdot}50 \times 10^{-2}$
0·5	$0{\cdot}37 \times 10^{-1}$	$0{\cdot}71 \times 10^{-1}$	$0{\cdot}43 \times 10^{-2}$	$0{\cdot}71 \times 10^{-1}$	$0{\cdot}43 \times 10^{-2}$	$0{\cdot}72 \times 10^{-1}$	$0{\cdot}43 \times 10^{-2}$	$0{\cdot}14 \times 10^{2}$	$0{\cdot}58 \times 10^{-2}$
0·6	$0{\cdot}62 \times 10^{-1}$	$0{\cdot}11 \times 10^{0}$	$0{\cdot}47 \times 10^{-2}$	$0{\cdot}11 \times 10^{0}$	$0{\cdot}47 \times 10^{-2}$	$0{\cdot}11 \times 10^{0}$	$0{\cdot}47 \times 10^{-2}$	$0{\cdot}18 \times 10^{2}$	$0{\cdot}68 \times 10^{-2}$
0·7	$0{\cdot}11 \times 10^{0}$	$0{\cdot}18 \times 10^{0}$	$0{\cdot}52 \times 10^{-2}$	$0{\cdot}18 \times 10^{0}$	$0{\cdot}53 \times 10^{-2}$	$0{\cdot}18 \times 10^{0}$	$0{\cdot}53 \times 10^{-2}$	$0{\cdot}22 \times 10^{2}$	$0{\cdot}84 \times 10^{-2}$
0·8	$0{\cdot}24 \times 10^{0}$	$0{\cdot}34 \times 10^{0}$	$0{\cdot}62 \times 10^{-2}$	$0{\cdot}34 \times 10^{0}$	$0{\cdot}63 \times 10^{-2}$	$0{\cdot}35 \times 10^{0}$	$0{\cdot}63 \times 10^{-2}$	$0{\cdot}28 \times 10^{2}$	$0{\cdot}11 \times 10^{-1}$
0·9	$0{\cdot}79 \times 10^{0}$	$0{\cdot}96 \times 10^{0}$	$0{\cdot}85 \times 10^{-2}$	$0{\cdot}95 \times 10^{0}$	$0{\cdot}88 \times 10^{-2}$	$0{\cdot}10 \times 10^{1}$	$0{\cdot}88 \times 10^{-2}$	$0{\cdot}41 \times 10^{2}$	$0{\cdot}16 \times 10^{-1}$
0·95	$0{\cdot}23 \times 10^{1}$	$0{\cdot}26 \times 10^{1}$	$0{\cdot}12 \times 10^{-1}$	$0{\cdot}25 \times 10^{1}$	$0{\cdot}12 \times 10^{-1}$	$0{\cdot}29 \times 10^{1}$	$0{\cdot}13 \times 10^{-1}$	$0{\cdot}59 \times 10^{2}$	$0{\cdot}23 \times 10^{-1}$
0·99	$0{\cdot}14 \times 10^{2}$	$0{\cdot}15 \times 10^{2}$	$0{\cdot}28 \times 10^{-1}$	$0{\cdot}11 \times 10^{2}$	$0{\cdot}29 \times 10^{-1}$	$0{\cdot}33 \times 10^{2}$	$0{\cdot}33 \times 10^{-1}$	$0{\cdot}13 \times 10^{3}$	$0{\cdot}53 \times 10^{-1}$

Table II. Results for $L/D = 1/1$

	Stokes 3D		Finite lub		Short lub		Long lub	
ε	F_Y	C	F_Y	C	F_Y	C	F_Y	C
0·1	$0{\cdot}67 \times 10^{1}$	$0{\cdot}37 \times 10^{-1}$	$0{\cdot}68 \times 10^{1}$	$0{\cdot}39 \times 10^{-1}$	$0{\cdot}95 \times 10^{1}$	$0{\cdot}38 \times 10^{-1}$	$0{\cdot}28 \times 10^{2}$	$0{\cdot}38 \times 10^{-1}$
0·2	$0{\cdot}14 \times 10^{2}$	$0{\cdot}38 \times 10^{-1}$	$0{\cdot}14 \times 10^{2}$	$0{\cdot}41 \times 10^{-1}$	$0{\cdot}20 \times 10^{2}$	$0{\cdot}39 \times 10^{-1}$	$0{\cdot}56 \times 10^{2}$	$0{\cdot}40 \times 10^{-1}$
0·3	$0{\cdot}22 \times 10^{2}$	$0{\cdot}39 \times 10^{-1}$	$0{\cdot}22 \times 10^{2}$	$0{\cdot}44 \times 10^{-1}$	$0{\cdot}32 \times 10^{2}$	$0{\cdot}41 \times 10^{-1}$	$0{\cdot}85 \times 10^{2}$	$0{\cdot}44 \times 10^{-1}$
0·4	$0{\cdot}31 \times 10^{2}$	$0{\cdot}42 \times 10^{-1}$	$0{\cdot}31 \times 10^{2}$	$0{\cdot}47 \times 10^{-1}$	$0{\cdot}49 \times 10^{2}$	$0{\cdot}45 \times 10^{-1}$	$0{\cdot}11 \times 10^{3}$	$0{\cdot}50 \times 10^{-1}$
0·5	$0{\cdot}42 \times 10^{2}$	$0{\cdot}46 \times 10^{-1}$	$0{\cdot}42 \times 10^{2}$	$0{\cdot}52 \times 10^{-1}$	$0{\cdot}72 \times 10^{2}$	$0{\cdot}50 \times 10^{-1}$	$0{\cdot}14 \times 10^{3}$	$0{\cdot}58 \times 10^{-1}$
0·6	$0{\cdot}57 \times 10^{2}$	$0{\cdot}52 \times 10^{-1}$	$0{\cdot}58 \times 10^{2}$	$0{\cdot}58 \times 10^{-1}$	$0{\cdot}11 \times 10^{3}$	$0{\cdot}60 \times 10^{-1}$	$0{\cdot}18 \times 10^{3}$	$0{\cdot}68 \times 10^{-1}$
0·7	$0{\cdot}78 \times 10^{2}$	$0{\cdot}61 \times 10^{-1}$	$0{\cdot}80 \times 10^{2}$	$0{\cdot}69 \times 10^{-1}$	$0{\cdot}18 \times 10^{3}$	$0{\cdot}78 \times 10^{-1}$	$0{\cdot}22 \times 10^{3}$	$0{\cdot}84 \times 10^{-1}$
0·8	$0{\cdot}11 \times 10^{3}$	$0{\cdot}78 \times 10^{-1}$	$0{\cdot}12 \times 10^{3}$	$0{\cdot}86 \times 10^{-1}$	$0{\cdot}35 \times 10^{3}$	$0{\cdot}12 \times 10^{0}$	$0{\cdot}28 \times 10^{3}$	$0{\cdot}11 \times 10^{0}$
0·9	$0{\cdot}21 \times 10^{3}$	$0{\cdot}12 \times 10^{0}$	$0{\cdot}21 \times 10^{3}$	$0{\cdot}13 \times 10^{0}$	$0{\cdot}10 \times 10^{4}$	$0{\cdot}27 \times 10^{0}$	$0{\cdot}41 \times 10^{3}$	$0{\cdot}16 \times 10^{0}$
0·95	$0{\cdot}33 \times 10^{3}$	$0{\cdot}18 \times 10^{0}$	$0{\cdot}35 \times 10^{3}$	$0{\cdot}19 \times 10^{0}$	$0{\cdot}29 \times 10^{4}$	$0{\cdot}68 \times 10^{0}$	$0{\cdot}59 \times 10^{3}$	$0{\cdot}23 \times 10^{0}$
0·99	$0{\cdot}82 \times 10^{3}$	$0{\cdot}42 \times 10^{0}$	$0{\cdot}80 \times 10^{3}$	$0{\cdot}42 \times 10^{0}$	$0{\cdot}33 \times 10^{5}$	$0{\cdot}68 \times 10^{1}$	$0{\cdot}13 \times 10^{4}$	$0{\cdot}53 \times 10^{0}$

Table III. Results for $L/D = 10/1$

	Stokes 3D		Finite lub		Short lub		Long lub	
ε	F_Y	C	F_Y	C	F_Y	C	F_Y	C
0·1	$0{\cdot}25 \times 10^{3}$	$0{\cdot}37 \times 10^{0}$	$0{\cdot}25 \times 10^{3}$	$0{\cdot}43 \times 10^{0}$	$0{\cdot}95 \times 10^{4}$	$0{\cdot}57 \times 10^{0}$	$0{\cdot}28 \times 10^{3}$	$0{\cdot}38 \times 10^{0}$
0·2	$0{\cdot}50 \times 10^{3}$	$0{\cdot}39 \times 10^{0}$	$0{\cdot}51 \times 10^{3}$	$0{\cdot}48 \times 10^{0}$	$0{\cdot}20 \times 10^{5}$	$0{\cdot}12 \times 10^{1}$	$0{\cdot}56 \times 10^{3}$	$0{\cdot}40 \times 10^{0}$
0·3	$0{\cdot}76 \times 10^{3}$	$0{\cdot}43 \times 10^{0}$	$0{\cdot}76 \times 10^{3}$	$0{\cdot}55 \times 10^{0}$	$0{\cdot}32 \times 10^{5}$	$0{\cdot}23 \times 10^{1}$	$0{\cdot}85 \times 10^{3}$	$0{\cdot}44 \times 10^{0}$
0·4	$0{\cdot}10 \times 10^{4}$	$0{\cdot}48 \times 10^{0}$	$0{\cdot}10 \times 10^{4}$	$0{\cdot}61 \times 10^{0}$	$0{\cdot}49 \times 10^{5}$	$0{\cdot}43 \times 10^{1}$	$0{\cdot}11 \times 10^{4}$	$0{\cdot}50 \times 10^{0}$
0·5	$0{\cdot}13 \times 10^{4}$	$0{\cdot}55 \times 10^{0}$	$0{\cdot}13 \times 10^{4}$	$0{\cdot}70 \times 10^{0}$	$0{\cdot}72 \times 10^{5}$	$0{\cdot}76 \times 10^{1}$	$0{\cdot}14 \times 10^{4}$	$0{\cdot}58 \times 10^{0}$
0·6	$0{\cdot}16 \times 10^{4}$	$0{\cdot}64 \times 10^{0}$	$0{\cdot}16 \times 10^{4}$	$0{\cdot}80 \times 10^{0}$	$0{\cdot}11 \times 10^{6}$	$0{\cdot}14 \times 10^{2}$	$0{\cdot}18 \times 10^{4}$	$0{\cdot}68 \times 10^{0}$
0·7	$0{\cdot}20 \times 10^{4}$	$0{\cdot}79 \times 10^{0}$	$0{\cdot}20 \times 10^{4}$	$0{\cdot}93 \times 10^{0}$	$0{\cdot}18 \times 10^{6}$	$0{\cdot}26 \times 10^{2}$	$0{\cdot}22 \times 10^{4}$	$0{\cdot}84 \times 10^{0}$
0·8	$0{\cdot}26 \times 10^{4}$	$0{\cdot}10 \times 10^{1}$	$0{\cdot}26 \times 10^{4}$	$0{\cdot}12 \times 10^{1}$	$0{\cdot}35 \times 10^{6}$	$0{\cdot}56 \times 10^{2}$	$0{\cdot}28 \times 10^{4}$	$0{\cdot}11 \times 10^{1}$
0·9	$0{\cdot}38 \times 10^{4}$	$0{\cdot}15 \times 10^{1}$	$0{\cdot}39 \times 10^{4}$	$0{\cdot}16 \times 10^{1}$	$0{\cdot}10 \times 10^{7}$	$0{\cdot}18 \times 10^{3}$	$0{\cdot}41 \times 10^{4}$	$0{\cdot}16 \times 10^{1}$
0·95	$0{\cdot}55 \times 10^{4}$	$0{\cdot}23 \times 10^{1}$	$0{\cdot}56 \times 10^{4}$	$0{\cdot}23 \times 10^{1}$	$0{\cdot}29 \times 10^{7}$	$0{\cdot}56 \times 10^{3}$	$0{\cdot}59 \times 10^{4}$	$0{\cdot}23 \times 10^{1}$
0·99	$0{\cdot}13 \times 10^{5}$	$0{\cdot}50 \times 10^{1}$	$0{\cdot}11 \times 10^{5}$	$0{\cdot}48 \times 10^{1}$	$0{\cdot}33 \times 10^{8}$	$0{\cdot}65 \times 10^{4}$	$0{\cdot}13 \times 10^{5}$	$0{\cdot}53 \times 10^{1}$

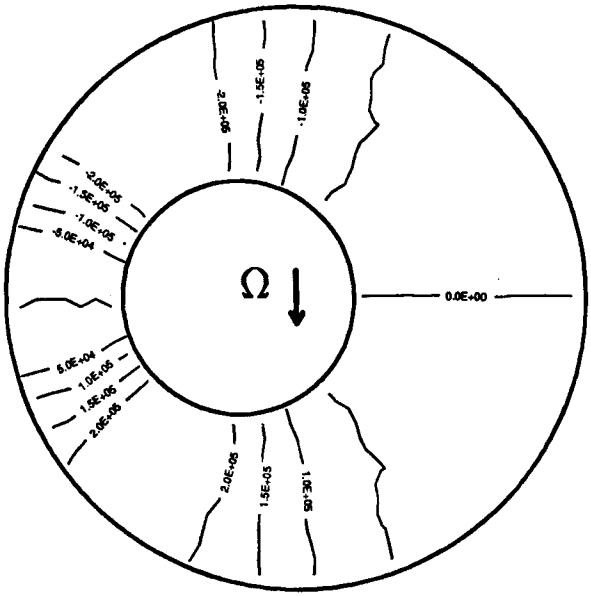

Figure 3. Pressure distribution (Pa) for $L/D = 1/10$, $\varepsilon = 0{\cdot}9$

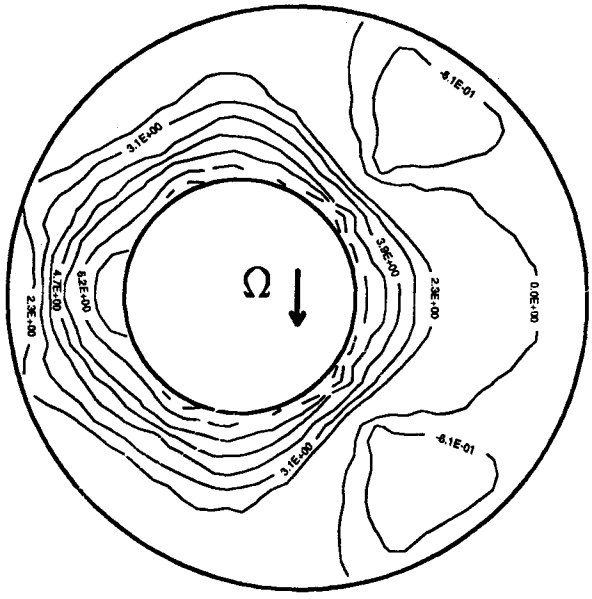

Figure 4. Circumferential velocity ($\mathrm{m\,s^{-1}}$) for $L/D = 1/10$, $\varepsilon = 0{\cdot}9$

We therefore decided to vary the strength of the line source about the journal so that it becomes a function of the circumferential co-ordinate, whilst still maintaining the correct total source strength Q. Specifically, a distribution is chosen so that fluid enters the bearing only at regions of negative pressure as calculated in the sourceless case. Again this creates a non-physical situation as

Table IV. Results for $L/D = 10/1$ with oil source

	Stokes flow with source		
ε	F_X	F_Y	C
0·1	$0{\cdot}35 \times 10^{-2}$	$0{\cdot}39 \times 10^{-2}$	$0{\cdot}38 \times 10^{-2}$
0·2	$0{\cdot}76 \times 10^{-2}$	$0{\cdot}84 \times 10^{-2}$	$0{\cdot}39 \times 10^{-2}$
0·3	$0{\cdot}13 \times 10^{-1}$	$0{\cdot}14 \times 10^{-1}$	$0{\cdot}40 \times 10^{-2}$
0·4	$0{\cdot}21 \times 10^{-1}$	$0{\cdot}23 \times 10^{-1}$	$0{\cdot}41 \times 10^{-2}$
0·5	$0{\cdot}34 \times 10^{-1}$	$0{\cdot}37 \times 10^{-1}$	$0{\cdot}43 \times 10^{-2}$
0·6	$0{\cdot}60 \times 10^{-1}$	$0{\cdot}62 \times 10^{-1}$	$0{\cdot}47 \times 10^{-2}$
0·7	$0{\cdot}12 \times 10^{0}$	$0{\cdot}11 \times 10^{0}$	$0{\cdot}52 \times 10^{-2}$
0·8	$0{\cdot}32 \times 10^{0}$	$0{\cdot}24 \times 10^{0}$	$0{\cdot}62 \times 10^{-2}$
0·9	$0{\cdot}17 \times 10^{1}$	$0{\cdot}79 \times 10^{0}$	$0{\cdot}85 \times 10^{-2}$

the pressure field is modified and areas of high pressure are built up around the source region. Other source distributions give similar results. This suggests that accurate modelling of the source will require an iterative scheme to deal with the interaction between the source and the pressure field. A more realistic model will be incorporated into future work.

7. DISCUSSION AND CONCLUSIONS

The work described in this paper is the first three-dimensional spectral solution to the Stokes flow problem for the journal bearing. A bipolar co-ordinate system is used to map the eccentric annulus onto a rectangular domain. To avoid the complication of free boundaries at the ends of the journal, all variables are periodically continued in the axial direction. The spectral discretization consists of expanding each variable as a triple tensor product of a Chebyshev series in the radial direction and Fourier series in both the circumferential and axial directions. The effect of an oil hole source in the journal is modelled by assuming a line source and specifying a suitable boundary condition on the radial velocity at the midpoint of the journal. To ensure conservation of mass, we periodically continue the source in terms of an infinite array of sources and sinks located along the axial direction.

In the absence of an oil source, results from the Stokes spectral solution are compared with those from lubrication theory. Good agreement is shown for those cases when the assumptions inherent in lubrication theory are satisfied. We also observed a recirculation region for the velocity field in the case of high eccentricity. This cannot be predicted by lubrication theory, but agrees with previous results for Stokes flow.[8] We therefore conclude that the formulation of the equations and the numerical methods are correct.

Inclusion of the fluid source is also a new feature, although physically meaningful results are not possible using the linear steady state scheme as reported in this paper. The accurate modelling of the source requires an iterative scheme in order to ensure that flow from the oil hole occurs only within regions where the pressure is below a certain threshold. A more realistic model for the fluid source will be incorporated into a time-dependent algorithm which will deal with the source–pressure interaction in a natural way at each time increment.

Work is proceeding on extending the analysis to the transient flow of non-Newtonian fluids. The proposed numerical scheme will use a pseudospectral discretization in space allied to a time-splitting projection method,[9] suitably extended for use in the non-Newtonian case. A preliminary

version of the time-dependent code is complete and is designed to cater for the generalized Newtonian, White–Metzner and I_2I_3 rheological models. The generalized Newtonian model will allow modelling of the shear-thinning behaviour of oils, which has a strong influence on the load-bearing characteristics of journal bearings. The White–Metzner model includes elasticity and variable viscosity. The tension-stiffening inelastic I_2I_3 model[10] will permit the isolation of effects due to shear and extensional viscosity. This will therefore clarify the role of extensional viscosity in bearing performance, an effect which has been the subject of debate for several years.

ACKNOWLEDGEMENTS

This work was funded by Shell Research Ltd., Thornton. We would like to thank Dr. T. W. Bates, Mr. J. Hutton and Professor K. Walters for useful discussions.

APPENDIX I: CALCULATION OF LOAD AND TORQUE FOR STOKES FLOW

The Cartesian components of the load and torque on the journal are given by (24)–(27). After substituting the field variable expansions (10), it is found that calculation of the load involves integrals of the form

$$a\sum_{k=0}^{K} T_k(\xi_J)\int_{-H}^{H}\begin{Bmatrix}\cos(n\pi z/L)\\ \sin(n\pi z/L)\end{Bmatrix}dz\int_0^{2\pi}\sum_{m=-M/2}^{M/2}\hat{\phi}_{lmn}\frac{\exp(im\eta)f(\eta)}{(\cosh\xi_J+\cos\eta)^2}d\eta, \tag{44}$$

where $f(\eta)$ is one of

$$f(\eta)=\begin{cases}1,\\ \cosh\xi_J\cos\eta,\\ \sinh\xi_J\sin\eta,\end{cases}$$

and those for the torque involve

$$aR_J\sum_{k=0}^{K} T_k(\xi_J)\int_{-H}^{H}\cos\left(\frac{n\pi z}{L}\right)dz\int_0^{2\pi}\sum_{m=-M/2}^{M/2}\hat{\phi}_{lmn}\frac{\exp(im\eta)}{(\cosh\xi_J+\cos\eta)}d\eta. \tag{45}$$

The component $T^{z\xi}$ is a sine series in z, which gives $F_Z=0$.

The integrals of the components of the cosine series are given by

$$\int_{-H}^{H}\cos\left(\frac{n\pi z}{L}\right)dz=\begin{cases}L, & n=0,\\ 2L/(n\pi)(-1)^{(n-1)/2}, & n \text{ odd},\\ 0, & \text{otherwise.}\end{cases}$$

Integration with respect to η may be performed by contour integration using the substitution $\zeta=\exp(i\eta)$. The expressions for **F** involve integrals of the form

$$I_m=\oint\frac{\zeta^m}{(\zeta-\zeta_1)^2(\zeta-\zeta_2)^2}d\zeta \quad (-M/2\leqslant m\leqslant M/2),$$

and those for C involve

$$J_m=\oint\frac{\zeta^m}{(\zeta-\zeta_1)(\zeta-\zeta_2)}d\zeta \qquad (-M/2\leqslant m\leqslant M/2),$$

where $\zeta_1=-\cosh\xi_J-\sqrt{(\cosh^2\xi_J-1)}$ and $\zeta_2=-\cosh\xi_J+\sqrt{(\cosh^2\xi_J-1)}$. By using the substitution $\omega=1/\zeta$, it may be seen that $I_m=I_{|m|+2}$, $m<0$ and $J_m=J_{|m|}$, $m<0$. The integrals have

single or double poles on the real axis at $\zeta = \zeta_1$ and $\zeta = \zeta_2$. We have that $\cosh \xi > 1$, so that $\zeta_1 < -1$ and $-1 < \zeta_2 < 1$; thus ζ_2 lies within the unit circle whereas ζ_1 is outside. The integrals are then calculated using Cauchy's residue theorem with only the poles at $\zeta = \zeta_2$ contributing.

APPENDIX II: CALCULATION OF LOAD FOR FINITE LUBRICATION THEORY

The Cartesian components of force on the journal are given by (32) and (33). After substituting in the expansion for pressure, the integrals become

$$\begin{Bmatrix} F_X \\ F_Y \end{Bmatrix} = \sum_{m=-M/2}^{M/2} \sum_{n=0}^{N} \hat{p}_{mn} \int_{-1}^{1} T_n(Z)\,\mathrm{d}Z \int_0^{2\pi} \exp(im\theta) \begin{Bmatrix} \cos\theta \\ \sin\theta \end{Bmatrix} R\,\mathrm{d}\theta.$$

The integrals may easily be calculated using the following standard expressions for the integrals of Chebyshev polynomials:

$$\int_{-1}^{1} T_n(Z)\,\mathrm{d}Z = \begin{cases} -2/(n^2-1), & n \text{ even}, \\ 0, & n \text{ odd}. \end{cases}$$

REFERENCES

1. T. W. Bates, B. Fantino, L. Launay and J. Frêne, 'Oil film thickness in an elastic connecting-rod bearing: comparison between theory and experiment', *Preprints ASME/STLE 1989 Tribology Conf., ASME Paper 89-AM-2B-1*, 1989.
2. M. Fortin and A. Fortin, 'A new approach for the FEM simulation of viscoelastic flows', *J. Non-Newtonian Fluid Mech.*, **32**, 295–310 (1989).
3. C. Canuto, M. Y. Hussaini, A. Quarteroni and T. A. Zang, *Spectral Methods in Fluid Dynamics*, Springer, New York, 1987.
4. C. Lanczos, *Applied Analysis*, Pitman, London, 1957.
5. L. N. Tao, 'On journal bearings of finite length', *J. Appl. Mech.*, **26**, 179–183 (1959).
6. A. Cameron, *The Principles of Lubrication*, Longmans, London, 1966.
7. R. I. Tanner, 'The estimation of bearing loads using Galerkin's method', *Int. J. Mech. Sci.*, **3**, 13–27 (1961).
8. A. Beris, R. C. Armstrong and R. A. Brown, 'Perturbation theory for viscoelastic fluids between eccentric rotating cylinders', *J. Non-Newtonian Fluid Mech.*, **13**, 109–148 (1983).
9. A. J. Chorin, 'Numerical solution of the Navier–Stokes equations', *Math. Comput.*, **22**, 745–762 (1968).
10. B. Debbaut, M. J. Crochet, H. Barnes and K. Walters, 'Extensional flows of inelastic fluids', *Proc. X Int. Congr. on Rheology*, Sydney, 1988.